Hindawi
Mathematical Problems in Engineering
Volume 2022, Article ID 1259131, 11 pages
https://doi.org/10.1155/2022/1259131

Research Article

Specific Surface Area Characterization of Spinel Ferrite Nanostructure Based Compounds for Photocatalysis and Other Applications Using Extreme Learning Machine Method

Miloud Souiyah,[1] Taoreed O. Owolabi,[2] Saibu Saliu,[2] Talal F. Qahtan,[3] Nahier Aldhafferi,[4] and Abdullah Alqahtani[4]

[1]*Department of Mechanical Engineering, College of Engineering, University of Hafr Al Batin, P.O. Box 1803, Hafr Al Batin 31991, Saudi Arabia*
[2]*Physics and Electronics Department, Adekunle Ajasin University, Akungba Akoko 342111, Ondo State, Nigeria*
[3]*Physics Department, College of Science and Humanities in Al-Kharj, Prince Sattam Bin Abdulaziz University, Al-Kharj 11942, Saudi Arabia*
[4]*Computer Information Systems Department, College of Computer Science and Information Technology, Imam Abdulrahman Bin Faisal University, Dammam 31441, Saudi Arabia*

Correspondence should be addressed to Taoreed O. Owolabi; owolabitaoreedolakunle@gmail.com

Received 11 February 2022; Revised 15 March 2022; Accepted 9 April 2022; Published 26 April 2022

Academic Editor: Ramin Ranjbarzadeh

Nanocrystalline spinel ferrite based compounds are technological driven materials with interesting potentials in photocatalysis for renewable energy generation, gas sensing for pollution control, magnetic drug delivery, rod antennas, storage media (high density) and supercapacitive materials, among others. Specific surface area of spinel ferrite based compounds contributes immensely to the application of this semiconductor in industrial domains. Experimental determination of specific surface area is laborious and costly and consumes appreciable time. Compositional substitutions in crystal structure effectively improve physical properties and enhance specific surface area through alteration of moment distribution between tetrahedral oxygen sites and octahedral coordination. With the aid of distorted lattice parameters due to compositional substitution and the spinel ferrite nanocrystallite size as model descriptors, this present work models the specific surface area of spinel ferrite nanomaterial through extreme learning machine (ELM) based intelligent modeling method. The developed sigmoid activation function-based ELM (S-ELM) model shows superior performance over genetic algorithm based support vector regression (GBSVR) and stepwise regression (STWR) models existing in the literature with performance improvement of 61.31% and 70.01%, respectively, using root mean square error performance metric. The significances of cobalt and lanthanum compositional substitution on the specific surface area of spinel ferrite nanomaterials were investigated using S-ELM model. Ease of implementation of S-ELM model as compared with the existing GBSVR model, coupled with the demonstrated improved performance and persistent closeness of its predictions with the experimental values, would be highly meritorious for quick and precise characterization of specific surface area of spinel ferrite nanomaterials for various desired applications.

1. Introduction

Spinel ferrite nanomaterials have recently attracted significant attention due to their unique and fascinating chemical, physical, magnetic, electrical, and optical properties [1, 2]. These properties are useful in a variety of technological advancements and applications, which include photocatalysis for renewable energy generation [3], cancer treatment [4], agents for antibacterial [5], electromagnets [6], gas sensors, biomedicine [7], switching devices [8], drug delivery [9, 10], magnetic recording [11], water splitting [12], magnetic resonance imaging [13], multilayer chip inductors

[14], supercapacitors [15], and spintronics, among others. Recent significant attention on nanomaterial based magnetic materials such as spinel ferrite nanomaterials can be attributed to their unique properties, which include the ability to adjust their optical, structural, magnetic, and electronic properties through doping as well as vacancy creation [16–19]. By altering the size, shape, manufacturing technique, dopant ions, and their concentration, various physical properties of a system containing nanoparticles can be changed [20–22]. Large specific surface area, excellent calcination ability, quantum confinement effect, and smaller crystal size render spinel ferrite based compound indispensable for many applications [23]. The size difference between a nanoparticle and its surface area is a vital aspect of nanotechnology since the smallest particle has a characteristic larger surface area. The inverse relation between the size of the nanoparticle and the surface area creates a dramatic change between the electronic structure of the bulk particle and that of the nanoparticle [24]. This work employs crystallite size and lattice distortion to model the specific surface area of spinel ferrite nanomaterial.

The ferrite family is classified as garnets, hexagonal, and spinel ferrite using crystal structure as a criterion [25]. Spinel ferrites are distinguished from other ferrite family members by their distinctive features, which have led to their deployment for many technological applications [9, 26, 27]. Spinel ferrites have the general chemical formula MFe_2O_4, with M denoting divalent ions such as Fe^{2+}, Co^{2+}, Zn^{2+}, Mg^{2+}, Mn^{2+}, and Ni^{2+}, among others [28]. There are two types of interstitial sites characterizing spinel crystal structure: the tetrahedral (A) and octahedral (B) sites. Spinel can further be grouped into three categories based on its crystal structure: inverse spinel, normal spinel, and complex spinel [29]. Fe(III) and M(II) occupy octahedral sites and tetrahedral, respectively, in normal spinel, and ZnFe2O4 is a typical example [30]. Because the interstitials of octahedral sites are often larger than those of tetrahedral sites, cations with lesser radii are more likely to be found at M sites. In contrast, those with larger radii are more likely to be found at Fe(III) sites. In inverse spinel, half of the Fe(III) is located in tetrahedral sites, whereas the M(II) and the remaining Fe(III) are found in octahedral sites, such as NiFe2O4 [31]. In complex spinel, M(II) and Fe(III) occupy tetrahedral and octahedral sites in a random order [12]. The features of spinel ferrites are compositional dependence, distribution of cations over sites available, and their preparation techniques [32]. To enhance their specific surface area for the desired application, several metal ions, including Ni, Gd, Sr, Zn, Co, Cd, etc., have been used to dope ferrite nanoparticles [25, 33–39], which alter the crystal lattice properties of the spinel ferrite at various nanoparticle sizes. The crystallite size and lattice parameter are utilized in this work to model specific surface area of spinel ferrite through an intelligent algorithm based on an extreme learning machine.

Extreme learning machine (ELM) is an enhanced version of a single hidden layer feedforward network with conventional potentials to adjust network weights (such as the output and input weights) and biases using traditional gradient descent approach [40, 41]. However, this approach consumes appreciable training time with characteristic less efficiency [42]. Extreme learning machine algorithm trains single hidden layer feedforward network using amazing trick in which the values of the biases and input weights are chosen randomly and arbitrarily. Hence, generalized inverse operation is purposely employed for output weight computation to minimize the generalized error while the system becomes simplified as linear systems [43]. Moreover, the ELM algorithm determines only the output weight with the circumvention of a descent-based approach known to be slow. Therefore, the computational techniques utilized by ELM algorithm lead to minimized training error, reduced computational time, and enhanced generalization ability due to minimization of output weight norm. These unique features of ELM algorithm have widened its application domain in varieties of fields and specialization [44–47]. The uniqueness of ELM algorithm is harnessed in this contribution to model specific surface area of spinel ferrite based compounds while the existing models in the literature determine specific surface area of the same compounds using stepwise regression (STWR) model and hybrid genetic algorithm based support vector regression (GBSVR) model [27]. The deficiency of STWR based model comes from its inability to account for nonlinearity between the descriptors and the measured specific surface area [27]. The existing GBSVR model shows better performance over STWR model due to its ability to adopt nonlinear mapping function for feature space data transformation coupled with hyperparameters optimization using genetic algorithm. The empirical risk minimization principle which formulates the mathematical background of ELM based model strengthens its universal approximation capacity over the structural risk minimization principle adopted by GBSVR model. The superiority of ELM has been demonstrated in this contribution by comparing the estimates of ELM based model with the existing models in the literature. The obtained performance enhancement of the ELM based model compared with other existing intelligent models in the literature is due to the universal approximation feature of ELM through Moore-Penrose generalized inverse implementation.

Novelties of the developed sigmoid activation function-based ELM (S-ELM) model over the existing models in the literature include the ease of implementation and better generalization capacity on the basis of performance metrics. The developed S-ELM model can be easily implemented using Excel or standard calculator while the implementation of the existing genetic algorithm based support vector regression (GBSVR) model [27] is restricted to MATLAB environment. S-ELM model has demonstrated enhanced performance of 4.67% (using correlation coefficient, CC), 5.28% (using mean absolute error, MAE), and 58.22% (using root mean square error, RMSE) over the existing GBSVR model [27] for training set of data samples while it achieves improved performance of 11.64% (using CC metric), 61% (using MAE metric), and 61.31% (using RMSE metric) for testing set of data samples. In the same vein, the developed S-ELM model shows performance improvement of 58.29% (using CC metric), 87.66% (using MAE metric), and 84.12% (using RMSE metric) over the existing stepwise regression

(STWR) model [27] on training set of samples while it demonstrates improved performance of 18.28% (using CC metric), 67.05% (using MAE metric), and 70.01% (using RMSE metric) for testing set of samples.

The roadmap of this work entails Section 2 (which presents the background of ELM, data acquisition, and computational methodology) and Section 3 (which shows and discusses results with comparison to the existing models in the literature).

2. Empirical Study and Computational Methodology

The mathematical background and extreme learning machine description are presented in this section. The section also includes the computational strategies and physical description of the dataset.

2.1. Extreme Learning Machine Intelligent Method. Extreme learning machine (ELM) is an intelligence based algorithm with single-layer feedforward network architecture and characteristic single hidden layer [40, 48, 49]. The algorithm randomly maps the hidden layer and ultimately assigns values for the biases and input weights with the goal of output weight computation using least-square approach. ELM algorithm conserves training time compared with the conventional backpropagation algorithm. At the same time, the characteristic stochastic choice of the input weights and the biases ensures universal approximation of the relationship between the target and descriptors. Consider a training set (ψ_r, S_r) of spinel nanoferrite based compounds of M number of samples in which the measured specific surface area of the magnetic semiconductor is defined as $S_r = [s_{r1}, s_{r2}, \ldots.., s_m]^T$ while the crystallite size and the lattice distortion which serve as the model descriptors are defined as $\psi_r = [\psi_{r1}, \psi_{r2}, \ldots..\psi_m]^T$. ELM algorithm models and approximates function linking (ψ_r, S_r) of spinel nanoferrite based compounds with σ hidden nodes and $\chi(\psi)$ activation function with an output presented in equation (1) [50].

$$\begin{aligned}\delta_r &= \sum_{r=1}^{\sigma} \varnothing_r \chi_r(\psi_i) \\ &= \sum_{r=1}^{\sigma} \varnothing_r \chi_r(\gamma_r \psi_r + \lambda_r),\end{aligned} \tag{1}$$

where $r = 1, 2, 3, \ldots, M$ $\gamma_r = [\gamma_{r1}, \gamma_{r2}, \ldots.., \gamma_m]^T$ is the weight vector linking hidden nodes with the input nodes, $\varnothing_r = [\varnothing_{r1}, \varnothing_{r2}, \ldots., \varnothing_m]^T$ is the weight vector joining hidden nodes with the output nodes, and λ_r represents the threshold of r hidden nodes. Supposing that the ELM algorithm approximates M-spinel nanoferrite based compound samples with minimum error, parameters $\varnothing_r$, γ_r, and λ_r exist, so that equation (2) is satisfied.

$$\sum_{r=1}^{\sigma} \varnothing_r \chi_r(\gamma_r \psi_r + \lambda_r) = S_{\text{pred}}, \tag{2}$$

where the estimated specific surface area using ELM algorithm is defined as S_{pred}. The matrix representation of the expression contained in equation (2) is shown in the following equation:

$$H\varphi = S_{\text{pred}}, \tag{3}$$

where $\mathbf{H} = \begin{bmatrix} \chi(\gamma_1\psi_1 + \lambda_1) & \cdots & \chi(\gamma_\sigma\psi_1 + \lambda_\sigma) \\ \vdots & \cdots & \vdots \\ \chi(\gamma_1\psi_M + \lambda_1) & \cdots & \chi(\gamma_\sigma\psi_M + \lambda_\sigma) \end{bmatrix}$,

$\boldsymbol{\varphi} = \begin{bmatrix} \varphi_1^{\mathbf{T}} \\ \vdots \\ \varphi_\sigma^{\mathbf{T}} \end{bmatrix}_{\boldsymbol{\sigma}\mathbf{xn}}$ and $\mathbf{S}_{\text{pred}} = \begin{bmatrix} \mathbf{S}_{\text{pred1}}^{\mathbf{T}} \\ \vdots \\ \mathbf{S}_{\text{pred}\sigma}^{\mathbf{T}} \end{bmatrix}_{\mathbf{Mxn}}$

The parameters γ_r and λ_r of the hidden layer are selected randomly, while the parameter $\varnothing_r$ of the output layer is computed through Moore-Penrose generalized inverse as presented in equation (4) [51].

$$\varnothing = H^T\left(HH^T\right)^{-1} S_{\text{pred}}. \tag{4}$$

2.2. Spinel Ferrite Nanomaterial Data Samples for Modeling and Simulation. The dataset samples utilized for modeling ELM based model that estimates specific surface area of doped spinel ferrite nanomaterials consist of the crystallite size and lattice parameter (along the crystallographic direction) as descriptors, while the desired target is the specific surface area after dopant incorporation. The entire samples for modeling are extracted from available forty different compounds of spinel ferrite nanomaterials in [52–58]. Introduction of dopants such as zinc into spinel ferrite nanomaterial crystal structure influences the specific surface area of the parent compound and further expands the crystal lattice without causing a disturbance on the lattice symmetry [59]. Similarly, crystallite size contributes to structural disorder on nanoparticle surface due to the significance of spin disorder as the ratio of the surface and volume is altered [60].

The correlation cross-plot between crystallite size, lattice parameter, and specific surface area is shown in Figure 1 purposely to deduce the trend of linear relationship between the specific surface area of spinel ferrite nanomaterials and the descriptors. The coefficients of a linear relationship between crystallite size and lattice parameter are −26.67% and −26.58%, respectively, which strongly indicates that the lattice constant and crystallite size are not linearly correlated with the specific surface area despite the established physical discretional relation [60–62]. To establish a relationship for specific surface area of spinel ferrite nanomaterial, hybrid genetic algorithm based support vector regression (GBSVR) and stepwise regression (STWR) models were proposed recently with acceptable performance metrics [27]. The present developed model based on ELM has characteristic ease of implementation and further shows superior performance as compared with the existing models.

2.3. Computational Method and Details. Extreme learning machine (ELM) based model for spinel ferrite nanomaterial specific surface area prediction was developed using

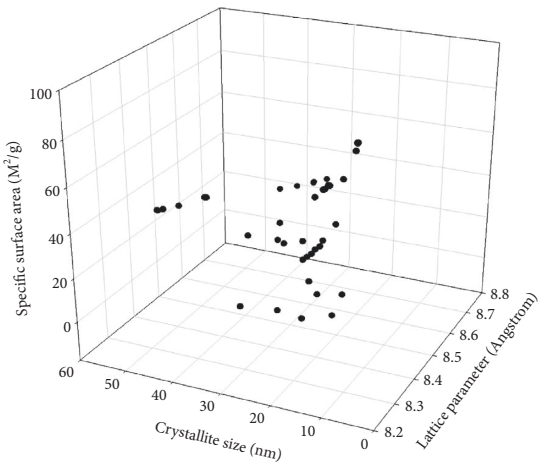

Figure 1: Three-dimensional cross-plot between the descriptors and specific surface area of doped spinel ferrite nanomaterial.

MATLAB computing environment. Randomization of forty samples of spinel ferrite nanomaterial based compounds was conducted while 4 : 1 ratio of data separation into training and testing phase followed. Randomization strengthens model efficiency and saves computational time in such a manner that model enjoys validation on approximated patterns during training phase. The generalization and predictive capacity of the proposed ELM based model were further enhanced through grid search approach of model parameters. The model parameter is the number of hidden nodes for different activation functions. However, these parameters could be optimized using metaheuristic algorithms [63–67], manual method [68], and grid search approach [69]. The choice of grid search approach in this work is due to a few numbers of model parameter (which is only the hidden node) which makes the choice of heuristic algorithm computationally noneconomical. Computational steps for the ELM based model are described as follows:

Step 1: *Initialization of Mersenne Twister Generator:* input weights and biases are generated using Mersenne Twister Generator within MATALAB. This pseudorandom generator further preserves the reproducibility of the model.

Step 2: *Number of hidden node optimization through a grid search approach for each of the chosen activation functions:* with the search space spanning between 1 and 100 for hidden node selection, one activation function was selected at a time from different available functions such as sigmoid function, triangular basis function, sine function, radial basis function, and hardlim function.

Step 3: *Hidden layer output matrix computation:* Deployment of training set of data on equation (3) yields the output matrix of the hidden layer.

Step 4: *Calculation of output weights connecting the hidden layer with the output layer:* Implementation of Moore-Penrose generalized inverse using equation (4) computes the output weights.

Step 5: *Validation stage and performance metrics computation:* The computed output matrix and the randomly generated input weights as well as the biases are employed using ELM operational principles to determine the specific surface area of spinel ferrite nanomaterial compounds that were excluded during training phase. The predictions of ELM based models developed were compared with the known experimental values of specific surface area while performance metrics such as mean absolute error (MAE), correlation coefficient (CC), and root mean square error (RMSE) were computed. The model with characteristic lowest value of MAE and RMSE was assigned the best model. The weights corresponding to the best model were also saved for subsequent deployment. The computational illustration of every step is presented in Figure 2.

3. Results and Discussion

The results of S-ELM model for specific surface area estimation is contained in this section. The comparison of the prediction strength of S-ELM model with the two existing models in the literature is further discussed.

3.1. Extreme Learning Based Functions for Specific Surface Area Prediction. The empirical equation generated through implementation of ELM algorithm for prediction of specific surface area of doped spinel ferrite nanomaterials is shown in equation (5). The obtained relation extends equation (4) with the sigmoid activation function.

$$S_{pred} = \sum_{r=1}^{\sigma} \varnothing_r / 1 + \exp\{-(\gamma_r \psi_i + \lambda_r)\}. \quad (5)$$

Several activation functions were explored while the sigmoid function demonstrated superior performance. The output weights ($\varnothing_r$), bias (λ_r), and input weights (γ_r) for each of the descriptors are presented in Table 1 for each of the hidden node. As presented in the table, the optimum number of hidden node is thirty-four. Ease of implementation of equation (5) contributes to its superiority (over the existing hybrid intelligent model in [27]) in addition to the enhanced performance demonstrated by the developed S-ELM model.

3.2. Model Performance Comparison. Performance of S-ELM model developed in this work is compared with GBSVR (2021) [27] and STWR (2021) [27] existing models in the literature and shown in Figure 3. Using mean absolute error (MAE) shown in Figure 3(a), S-ELM model outperforms GBSVR (2021) and STWR (2021) model with performance improvement of 5.28% and 87.66%, respectively, while percentage improvements of 4.67% and 58.30% were, respectively, obtained using correlation coefficient (CC) as presented in Figure 3(b).

Similar comparison on the basis of root mean square error (RMSE) presented in Figure 3(c) shows performance improvement of 58.21% and 84.12%, respectively. During

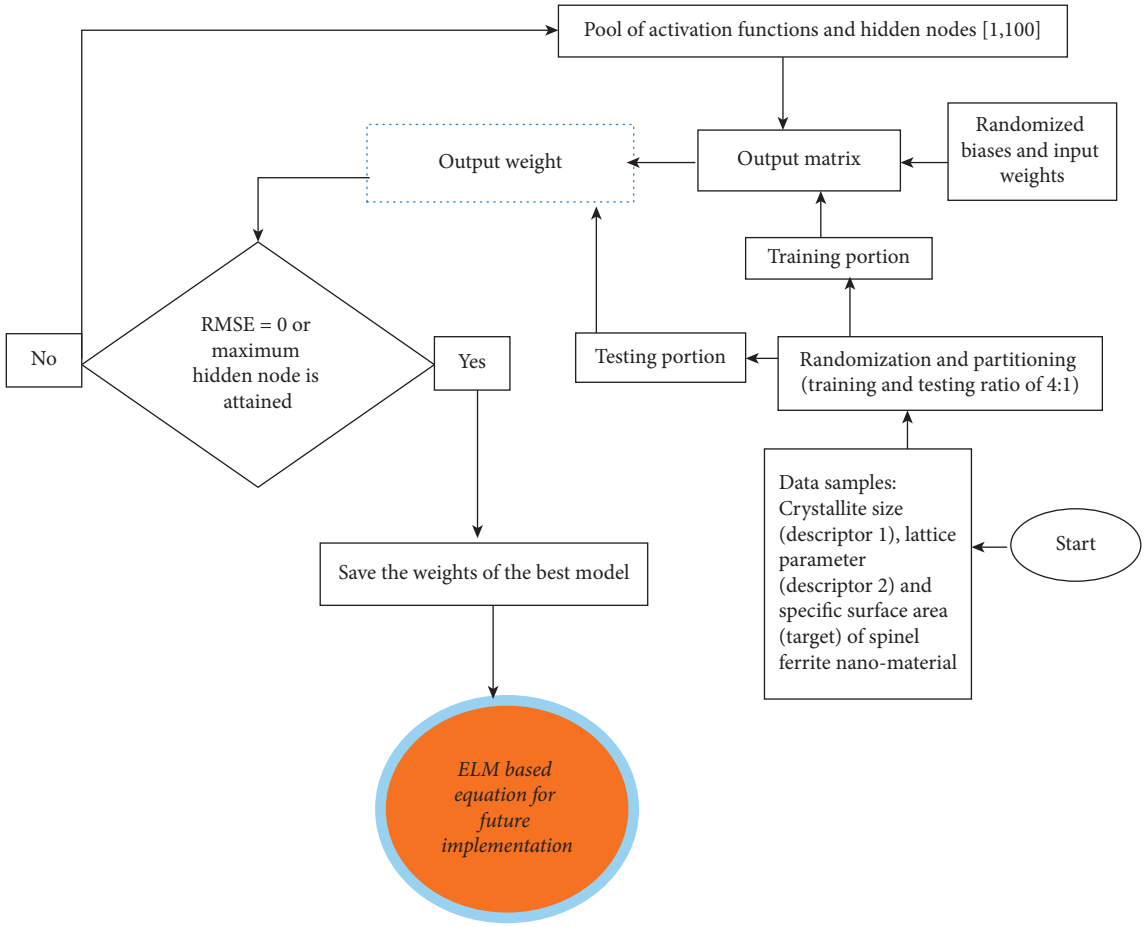

Figure 2: ELM based model flowchart for specific surface area of spinel ferrite nanomaterial estimation.

testing stage of model development, S-ELM model outperforms GBSVR (2021) [27] and STWR (2021) [27] existing models with performance improvement of 61.0% and 67.06% on the basis of MAE presented in Figure 3(d), and 11.64% and 18.28% on the basis of CC presented in Figure 3(e), 61.31% and 70.1% on the basis of RMSE presented in Figure 3(f), respectively. Table 2 presents the values of each of the parameters' measuring performance as well as the performance superiority of the present S-ELM model over the existing models.

3.3. Predictions of the Present and Existing Models. The results of the influence of different dopants on specific surface area of spinel ferrite nanomaterials are presented in Table 3. Cobalt-based spinel ferrite shows enhanced surface area at various crystallite sizes of nanomaterials with reduced crystal lattice constant [52]. The variation in lattice constant which manifested into enhanced surface area is due to smaller ionic radius of cobalt as compared with the copper ions. Site preference for each of the metal ions results in enhanced surface area, as can be observed in manganese, copper, and codoping systems presented in Table 3. The significances/effects of other different kinds of dopants on surface area of spinel ferrite nanomaterials are presented in Table 3. The estimates of S-ELM model show consistent and persistent closeness with the measured values compared with the estimates of the two existing GBSVR (2021) and STWR (2021) models. The precision characterizing the developed S-ELM model can also be inferred from the lowest MAE value and highest CC value for the entire spinel ferrite nanomaterials presented in Table 3. The universal approximation power of ELM algorithm through Moore-Penrose generalized inverse implementation contributes immensely to its superior performance. The result of yttrium substitution for cadmium in $Cd_{1-x}Y_xFe_2O_4$ ferrite compound is presented in Table 3. There is alteration in cation distribution since yttrium and cadmium ions occupy the tetrahedral site during the substitution while the octahedral site is occupied by the iron [54]. The observed ions distribution leads to gradual reduction in the value of the compound's specific surface area as the yttrium concentration increases while the results of the developed S-ELM model capture the majority of the observed experimental trends. The estimated specific surface area for gadolinium (rare Earth metal) substitution in spinel ferrite compound using S-ELM model is also presented in Table 3. Gadolinium ions in lattice structure of $Zn_{0.5}Mg_{0.5}Fe_{2-x}Gd_xO_4$ ferrite cause interstitial site stretching in octahedral and tetrahedral sublattice and further promote cations redistribution which alters the specific surface area of the compound [55]. The empirical risk minimization principle governing the employed ELM

Table 1: ELM parameters for empirical equation implementation.

Hidden node (r)	$\varnothing_r$	λ_r	γ_r (lattice parameter)	γ_r (crystallite size)
1	−0.62274	−0.09551	0.662722	$-2.2E+09$
2	0.945422	0.888646	0.396684	$5E+12$
3	−0.57982	0.29738	0.507116	$-4.8E+07$
4	−0.8383	−0.51232	0.65382	$-3E+13$
5	−0.14263	−0.9731	0.825833	$-9.3E+11$
6	0.732903	−0.37844	0.361	−1669932
7	−0.04152	0.070403	0.559194	425195.2
8	0.445617	−0.23035	0.746379	5102536
9	−0.68086	−0.28236	0.693861	$1.38E+11$
10	0.240922	−0.3114	0.324664	$-3E+08$
11	0.250907	0.186269	0.344454	$1.54E+10$
12	0.17992	−0.55345	0.807188	$-2.9E+09$
13	0.935471	0.408186	0.118581	$-1.2E+13$
14	−0.4163	0.231036	0.123533	26047114
15	0.020411	0.840614	0.373485	$-6.4E+12$
16	−0.56299	0.54586	0.000409	$-5.7E+08$
17	0.085264	0.700882	0.376104	$-4.3E+12$
18	−0.36751	−0.1255	0.329068	$1.06E+09$
19	0.577621	−0.22523	0.785514	434085.8
20	0.247755	0.230884	0.351277	$1.09E+10$
21	0.437797	−0.95321	0.661203	$1.99E+11$
22	−0.71626	−0.62271	0.015629	$-1.1E+13$
23	−0.77069	0.949419	0.086171	$-1.7E+10$
24	0.911439	0.232516	0.903004	$3.4E+12$
25	−0.34473	−0.20198	0.030566	$4.1E+10$
26	0.351874	−0.82816	0.117889	$-7.1E+11$
27	0.956593	0.165212	0.633875	$1.81E+10$
28	−0.9117	−0.42496	0.101884	$8.58E+12$
29	0.716314	0.082483	0.388419	$-4.1E+09$
30	−0.25616	−0.87667	0.23045	$-1.1E+12$
31	−0.81234	0.208952	0.366493	−98509.6
32	0.89921	0.692168	0.754947	$5.48E+12$
33	0.867543	−0.79842	0.374596	$5.58E+08$
34	0.988284	0.566743	0.021894	$8.37E+12$

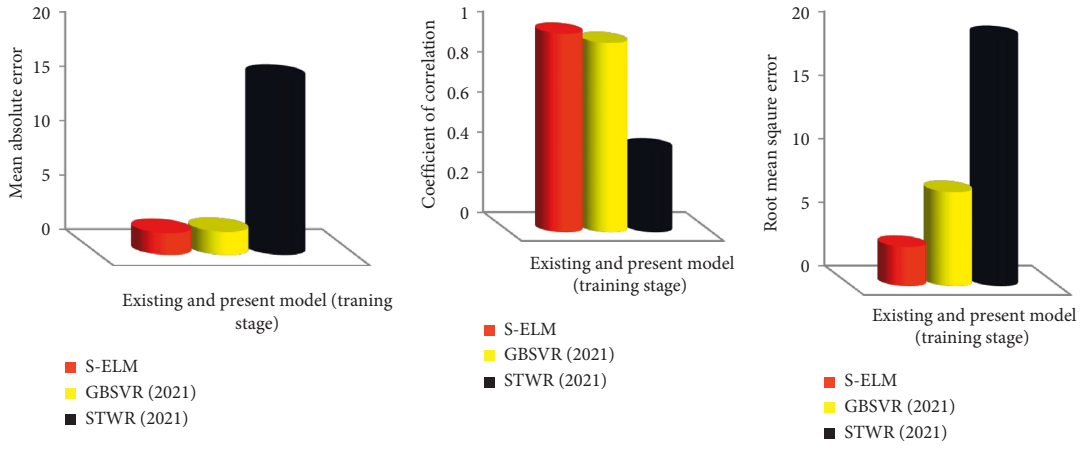

(a) (b) (c)

Figure 3: Continued.

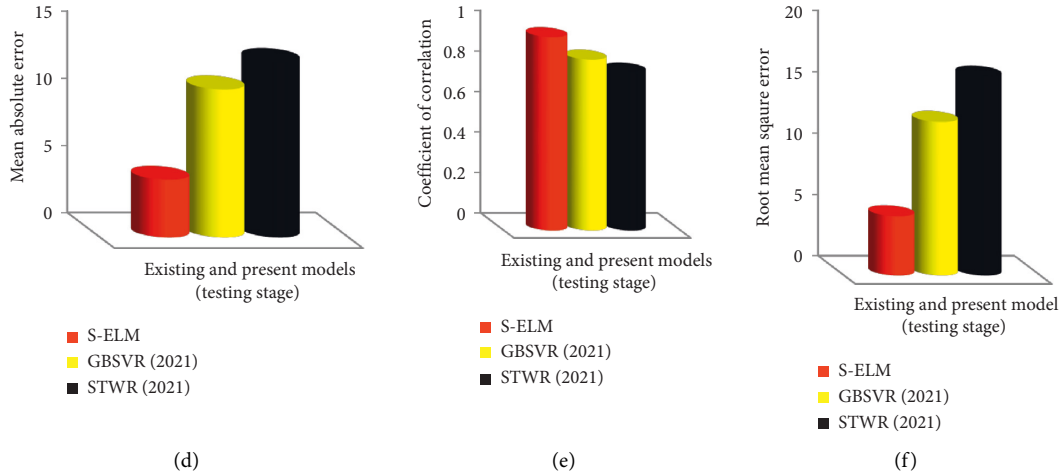

Figure 3: Comparison of S-ELM model and GBSVR (2021) and STWR (2021) models: (a) based on a mean absolute error on training dataset; (b) based on coefficient of correlation on training dataset; (c) based on root mean square error on training dataset; (d) based on mean absolute error on testing dataset; (e) based on coefficient of correlation on testing dataset; (f) based on root mean square error on testing dataset.

Table 2: Comparison of model performance as well as the performance superiority.

	Training			Testing		
	CC	MAE	RMSE	CC	MAE	RMSE
S-ELM	0.9902	2.0029	3.1181	0.9566	4.3021	4.8494
GBSVR (2021) [27]	0.9440	2.1146	7.4631	0.8452	11.0318	12.535
STWR (2021) [27]	0.4130	16.2313	19.6192	0.7817	13.0592	16.2186
% superiority of S-ELM over GBSVR	4.6726	5.2819	58.2192	11.6454	61.0032	61.3127
% superiority of S-ELM over STWR	58.2962	87.6602	84.1066	18.2793	67.0573	70.0991

Table 3: Specific surface area of different spinel ferrite based nanomaterials as obtained from experimental values and developed S-ELM model as well as the existing GBSVR (2021) and STWR (2021) models. All values of specific surface area are measured in (M^2/g).

Spinel ferrite nanomaterial	Measured specific surface area	S-ELM	Residual	GA-SVR (2021)	Residual	SWR (2021)	Residual
$CoFe_2O_4$	23.500 [52]	23.598	0.098	23.600	0.100	46.054	22.554
$CuFe_2O_4$	8.900 [52]	3.754	5.146	9.000	0.100	48.881	39.981
$MnFe_2O_4$	0.400 [52]	1.035	0.635	36.117	35.717	34.528	34.128
$MN_{0.4}Co_{0.6}Fe_2O_4$	11.900 [52]	11.906	0.006	12.000	0.100	35.832	23.932
$Mn_{0.4}Co_{0.4}Cu_{0.2}Fe_2O_4$	8.800 [52]	10.793	1.993	28.379	19.579	34.361	25.561
$Mn_{0.4}Co_{0.2}Cu_{0.4}Fe_2O_4$	4.000 [52]	4.770	0.770	4.100	0.100	38.662	34.662
$MN_{0.4}Cu_{0.6}Fe_2O_4$	1.400 [52]	6.734	5.334	1.500	0.100	34.932	33.532
$Mg_{0.25}Ni_{0.15}Cu_{0.25}Co_{0.35}Fe_{2-x}La_xO_4$ ($x = 0$)	40.047 [53]	40.656	0.609	40.046	0.001	27.126	12.921
$Mg_{0.25}Ni_{0.15}Cu_{0.25}Co_{0.35}Fe_{2-x}La_xO_4$ ($x = 0.03$)	43.503 [53]	46.320	2.817	40.436	3.067	29.593	13.910
$Mg_{0.25}Ni_{0.15}Cu_{0.25}Co_{0.35}Fe_{2-x}La_xO_4$ ($x = 0.06$)	48.562 [53]	51.320	2.758	48.462	0.100	32.158	16.404
$Mg_{0.25}Ni_{0.15}Cu_{0.25}Co_{0.35}Fe_{2-x}La_xO_4$ ($x = 0.09$)	49.071 [53]	44.652	4.419	46.434	2.637	32.337	16.734
$Mg_{0.25}Ni_{0.15}Cu_{0.25}Co_{0.35}Fe_{2-x}LaxO_4$ ($x = 0.12$)	40.067 [53]	33.590	6.477	40.167	0.100	28.269	11.798
$Mg_{0.25}Ni_{0.15}Cu_{0.25}Co_{0.35}Fe_{2-x}La_xO_4$ ($x = 0.15$)	39.361 [53]	43.102	3.741	39.461	0.100	27.573	11.788
$Cd_{1-x}Y_xFe_2O_4 (x = 0)$ [54]	32.180 [54]	32.539	0.359	32.280	0.100	19.719	12.461
$Cd_{1-x}Y_xFe_2O_4 (x = 0.125)$	29.900 [54]	37.289	7.389	30.000	0.100	25.880	4.020
$Cd_{1-x}Y_xFe_2O_4 (x = 0.250)$	30.420 [54]	22.383	8.037	30.320	0.100	25.393	5.027

Table 3: Continued.

Spinel ferrite nanomaterial	Measured specific surface area	S-ELM	Residual	GA-SVR (2021)	Residual	SWR (2021)	Residual
$Cd_{1-x}Y_xFe_2O_4 (x = 0.375)$	25.440 [54]	25.637	0.197	25.540	0.100	39.862	14.422
$Cd_{1-x}Y_xFe_2O_4 (x = 0.5)$	28.740 [54]	28.238	0.502	28.840	0.100	31.757	3.017
$Zn_{0.5}Mg_{0.5}Fe_2O_4$	24.860 [55]	23.746	1.114	40.292	15.432	35.567	10.707
$Zn_{0.5}Mg_{0.5}Fe_{1.98}Gd_{0.02}O_4$	25.524 [55]	24.207	1.317	38.006	12.482	34.715	9.191
$Zn_{0.5}Mg_{0.5}Fe_{1.96}Gd_{0.04}O_4$	26.756 [55]	26.820	0.064	26.856	0.100	34.053	7.297
$Zn_{0.5}Mg_{0.5}Fe_{1.94}Gd_{0.06}O_4$	28.250 [55]	32.117	3.867	28.350	0.100	33.331	5.081
$Zn_{0.5}Mg_{0.5}Fe_{1.92}Gd_{0.08}O_4$	29.497 [55]	32.109	2.612	29.480	0.017	32.559	3.062
$Zn_{0.5}Mg_{0.5}Fe_{2-x}Gd_xO_4 (x = 0.1)$	31.837 [55]	30.688	1.150	31.937	0.100	31.884	0.047
$Zn_{0.5}Co_{0.05}La_xFe_{2-x}O_4 (x = 0)$	33.300 [56]	27.141	6.159	40.083	6.783	34.896	1.596
$Zn_{0.5}Co_{0.05}La_xFe_{2-x}O_4 (x = 0.025)$	55.500 [56]	54.887	0.613	55.400	0.100	38.741	16.759
$Zn_{0.5}Co_{0.05}La_xFe_{2-x}O_4 (x = 0.05)$	58.800 [56]	50.000	8.800	58.700	0.100	38.286	20.514
$Zn_{0.5}Co_{0.05}La_xFe_{2-x}O_4 (x = 0.075)$	59.200 [56]	53.848	5.352	59.300	0.100	38.330	20.870
$Zn_{0.5}Co_{0.05}La_xFe_{2-x}O_4 (x = 0.1)$	60.900 [56]	60.363	0.537	39.996	20.904	38.324	22.576
$Zn_{0.5}Co_{0.05}La_xFe_{2-x}O_4 (x = 0.125)$	60.800 [56]	61.102	0.302	43.691	17.109	38.333	22.467
$Co_{0.9}Ni_{0.1}Fe_2O_4$	41.800 [57]	41.418	0.382	41.700	0.100	34.085	7.715
$Co_{0.7}Ni_{0.3}Fe_2O_4$	64.700 [57]	64.691	0.009	64.600	0.100	39.379	25.321
$Co_{0.5}Ni_{0.5}Fe_2O_4$	79.500 [57]	79.488	0.012	79.400	0.100	45.148	34.352
$Co_{0.3}Ni_{0.7}Fe_2O_4$	85.200 [57]	85.195	0.005	85.100	0.100	51.574	33.626
$Co_{0.1}Ni_{0.9}Fe_2O_4$	92.700 [57]	92.695	0.005	92.600	0.100	73.049	19.651
$Cu_{0.5}Cd_{0.25}Co_{0.25}Fe_2O_4$	25.349 [58]	29.527	4.178	25.449	0.100	31.361	6.012
$Cu_{0.5}Cd_{0.25}Co_{0.25}Fe_{1.9875}O_4$	26.311 [58]	23.605	2.706	34.640	8.329	32.075	5.764
$Cu_{0.5}Cd_{0.25}Co_{0.25}Fe_{1.975}O_4$	29.266 [58]	29.984	0.718	40.431	11.165	31.776	2.510
$Cu_{0.5}Cd_{0.25}Co_{0.25}Fe_{1.9625}O_4$	37.102 [58]	35.063	2.040	37.002	0.100	33.245	3.857
$Cu_{0.5}Cd_{0.25}Co_{0.25}Fe_{1.95}O_4$	41.808 [58]	47.090	5.282	41.708	0.100	33.760	8.049
		MAE	2.463		3.898		15.597
		CC	0.986		0.916		0.461

algorithm strengthens its universal approximation capacity and translates to improved performance as compared with structural risk minimization principle utilized by the existing GBSVR model. The deviations between the estimates of S-ELM model and the measured values can be reduced further through implementation of advanced intelligent algorithms such as sensitivity linear learning method of neural networks, metaheuristically optimized extreme learning method, and gravitational search algorithm based support vector regression, among others.

4. Conclusion

Extreme learning machine (S-ELM) based model was developed for predicting the specific surface area of spinel ferrite based nanomaterials using the lattice distortion (due to the incorporated dopants) and the size of nanoparticle crystallite as descriptors. S-ELM model has demonstrated enhanced performance of 4.67% (using CC metric), 5.28% (using MAE), and 58.22% (using RMSE metric) over the existing GBSVR model for training set of data samples while it achieves improved performance of 11.64% (using CC metric), 61% (using MAE metric), and 61.31% (using RMSE metric) for testing set of data samples. Similarly, S-ELM model shows performance improvement of 58.29% (using CC metric), 87.66% (using MAE metric), and 84.12% (using RMSE metric) over the existing STWR model on training set of samples while it demonstrates improved performance of 18.28% (using CC metric), 67.05% (using MAE metric), and 70.01% (using RMSE metric) for testing set of samples. The developed S-ELM model investigates the influence of cobalt, yttrium, magnesium, nickel, and cadmium on specific surface areas of spinel ferrite nanomaterials. Aside from the ease of implementation of S-ELM model, its enhanced performance further contributes to its uniqueness. The precision demonstrated by S-ELM model would strengthen quick, efficient, and precise characterization of the specific surface area of spinel ferrite based compounds with circumvention of time demanding experimental procedures. Advanced intelligent algorithms such as sensitivity linear learning method of neural networks, metaheuristically optimized extreme learning method, and gravitational search algorithm based support vector regression could be developed for spinel ferrite specific surface area modeling in future works.

Data Availability

The needed raw data for reproducing the presented findings are available in the cited references in Section 2.2 of the manuscript.

Conflicts of Interest

The authors declare no conflicts of interest.

Acknowledgments

This research work was funded by the contributing authors and no external fund was received.

References

[1] P. Lavanya Rathi and S. Deepa, "Structural, magnetic, thermal and optical properties of Sn2+ cation doped magnetite nanoparticles," *Ceramics International*, vol. 46, no. 3, pp. 2969–2978, 2020.

[2] Y. Slimani, B. Unal, M. A. Almessiere et al., "Investigation of structural and physical properties of Eu3+ ions substituted Ni0.4Cu0.2Zn0.4Fe2O4 spinel ferrite nanoparticles prepared via sonochemical approach," *Results in Physics*, vol. 17, Article ID 103061, 2020.

[3] K. K. Kefeni and B. B. Mamba, "Photocatalytic application of spinel ferrite nanoparticles and nanocomposites in wastewater treatment: Review," *Sustainable Materials and Technologies*, vol. 23, Article ID e00140, 2020.

[4] K. K. Kefeni, T. A. M. Msagati, T. T. Nkambule, and B. B. Mamba, "Spinel ferrite nanoparticles and nanocomposites for biomedical applications and their toxicity," *Materials Science and Engineering: C*, vol. 107, Article ID 110314, 2020.

[5] A. Samavati and A. F. Ismail, "Antibacterial properties of copper-substituted cobalt ferrite nanoparticles synthesized by co-precipitation method," *Particuology*, vol. 30, pp. 158–163, 2017.

[6] A. Sharma, K. M. Batoo, E. H. Raslan, S. F. Adil, and G. Kumar, "Structural and magnetic study of Mn0.5Zn0.5CuxFe2-xO4 nanoferrites synthesized via solution combustion method," *Vacuum*, vol. 157, pp. 422–427, 2018.

[7] K. Srinivasan, N. Zebardast, P. Krishnamurthy et al., "Comparison of new visual disturbances after superior versus nasal/temporal laser peripheral iridotomy," *Ophthalmology*, vol. 125, no. 3, pp. 345–351, 2018.

[8] A. Sharma, K. M. Batoo, E. H. Raslan, and G. Kumar, "Effect of chromium ions on the structural, magnetic, and optical properties of manganese-zinc ferrite nanoparticles," *Journal of Materials Science: Materials in Electronics*, vol. 31, no. 19, Article ID 16959, 2020.

[9] S. B. Kale, S. B. Somvanshi, M. N. Sarnaik, S. D. More, S. J. Shukla, and K. M. Jadhav, "Enhancement in surface area and magnetization of CoFe2O4 nanoparticles for targeted drug delivery application," *AIP Conference Proceedings*1953 pages, 2018.

[10] N. N. Al-Rawi, B. A. Anwer, N. H. Al-Rawi, A. T. Uthman, and I. S. Ahmed, "Magnetism in drug delivery: the marvels of iron oxides and substituted ferrites nanoparticles," *Saudi Pharmaceutical Journal*, vol. 28, no. 7, pp. 876–887, 2020.

[11] R. Sharma, P. Thakur, M. Kumar et al., "Improvement in magnetic behaviour of cobalt doped magnesium zinc nanoferrites via co-precipitation route," *Journal of Alloys and Compounds*, vol. 684, pp. 569–581, 2016.

[12] K. K. Kefeni, B. B. Mamba, and T. A. M. Msagati, "Application of spinel ferrite nanoparticles in water and wastewater treatment: a review," *Separation and Purification Technology*, vol. 188, pp. 399–422, 2017.

[13] N. Alghamdi, J. Stroud, M. Przybylski et al., "Structural, magnetic and toxicity studies of ferrite particles employed as contrast agents for magnetic resonance imaging thermometry," *Journal of Magnetism and Magnetic Materials*, vol. 497, 2019.

[14] T. Krishnaveni, B. R. Kanth, V. S. R. Raju, and S. R. Murthy, "Fabrication of multilayer chip inductors using Ni-Cu-Zn ferrites," *Journal of Alloys and Compounds*, vol. 414, no. 1, pp. 282–286, 2006.

[15] S. S. Kumbhar, M. A. Mahadik, V. S. Mohite, Y. M. Hunge, K. Y. Rajpure, and C. H. Bhosale, "Effect of Ni content on the structural, morphological and magnetic properties of spray deposited Ni-Zn ferrite thin films," *Materials Research Bulletin*, vol. 67, pp. 47–54, 2015.

[16] E. Petrova, D. Kotsikau, and V. Pankov, "Structural characterization and magnetic properties of sol-gel derived Zn x Fe 3-x O 4 nanoparticles," *Journal of Magnetism and Magnetic Materials*, vol. 378, pp. 429–435, 2015.

[17] D. Kotsikau, M. Ivanovskaya, V. Pankov, and Y. Fedotova, "Structure and magnetic properties of manganese-zinc-ferrites prepared by spray pyrolysis method," *Solid State Sciences*, vol. 39, pp. 69–73, 2015.

[18] M. Satalkar, S. N. Kane, M. Kumaresavanji, and J. P. Araujo, "On the role of cationic distribution in determining magnetic properties of Zn 0.7-x Ni x Mg 0.2 Cu 0.1 Fe 2 O 4 nano ferrite," *Materials Research Bulletin*, vol. 91, pp. 14–21, 2017.

[19] K. Kombaiah, J. J. Vijaya, L. J. Kennedy et al., "Effect of Cd2+ concentration on ZnFe2O4 nanoparticles on the structural, optical and magnetic properties," *Optik*, vol. 135, pp. 190–199, 2017.

[20] D. Carta, M. F. Casula, A. Falqui et al., "A structural and magnetic investigation of the inversion degree in ferrite nanocrystals MFe2O4(M = Mn, Co, Ni)," *Journal of Physical Chemistry C*, vol. 113, no. 20, pp. 8606–8615, 2009.

[21] S. B. Darling and S. D. Bader, "A materials chemistry perspective on nanomagnetism," *Journal of Materials Chemistry*, vol. 15, no. 39, pp. 4189–4195, 2005.

[22] D. Chaudhary and B. Kumar, "Cost optimized hybrid genetic-gravitational search algorithm for load scheduling in cloud computing," *Applied Soft Computing*, vol. 83, Article ID 105627, 2019.

[23] M. A. Almessiere, A. Demir Korkmaz, Y. Slimani, M. Nawaz, S. Ali, and A. Baykal, "Magneto-optical properties of rare earth metals substituted Co-Zn spinel nanoferrites," *Ceramics International*, vol. 45, no. 3, pp. 3449–3458, 2019.

[24] D. S. Mathew and R. S. Juang, "An overview of the structure and magnetism of spinel ferrite nanoparticles and their synthesis in microemulsions," *Chemical Engineering Journal*, vol. 129, no. 1, pp. 51–65, 2007.

[25] G. L. Jadhav, S. D. More, C. M. Kale, and K. M. Jadhav, "Effect of magnesium substitution on the structural, morphological, optical and wettability properties of cobalt ferrite thin films," *Physica B: Condensed Matter*, vol. 555, pp. 61–68, 2019.

[26] M. Houshiar, F. Zebhi, Z. J. Razi, A. Alidoust, and Z. Askari, "Synthesis of cobalt ferrite (CoFe2O4) nanoparticles using combustion, coprecipitation, and precipitation methods: a comparison study of size, structural, and magnetic properties," *Journal of Magnetism and Magnetic Materials*, vol. 371, pp. 43–48, 2014.

[27] T. O. Owolabi, T. A. Saleh, O. Olusayo, M. Souiyah, and O. E. Oyeneyin, "Modeling the specific surface area of doped spinel ferrite nanomaterials using hybrid intelligent computational method," *Journal of Nanomaterials*, vol. 2021, Article ID 9677423, 2021.

[28] S. Dasgupta, B. Das, Q. Li et al., "Toward on-and-off magnetism: reversible electrochemistry to control magnetic phase transitions in spinel ferrites," *Advanced Functional Materials*, vol. 26, no. 41, pp. 7507–7515, 2016.

[29] Q. Zhao, Z. Yan, C. Chen, and J. Chen, "Spinels: controlled preparation, oxygen reduction/evolution reaction application, and beyond," *Chemical Reviews*, vol. 117, no. 15, Article ID 10121, 2017.

[30] Y. Li, Y. Li, X. Xu et al., "Structural disorder controlled oxygen vacancy and photocatalytic activity of spinel-type minerals: a case study of ZnFe2O4," *Chemical Geology*, vol. 504, pp. 276–287, 2019.

[31] M. Nawaz, A. Shahzad, K. Tahir et al., "Photo-Fenton reaction for the degradation of sulfamethoxazole using a multi-walled carbon nanotube-NiFe2O4 composite," *Chemical Engineering Journal*, vol. 382, Article ID 123053, 2020.

[32] A. Sankaramahalingam and J. B. Lawrence, "Structural, optical, and magnetic properties of MgFe2O4 synthesized with addition of copper," *Synthesis and Reactivity in Inorganic Metal-Organic and Nano-Metal Chemistry*, vol. 42, no. 1, pp. 121–127, 2012.

[33] Z. K. Heiba, M. B. Mohamed, H. H. Hamdeh, and M. A. Ahmed, "Structural analysis and cations distribution of nanocrystalline Ni1−Zn Fe1.7Ga0.3O4," *Journal of Alloys and Compounds*, vol. 618, pp. 755–760, 2015.

[34] M. Satalkar, S. N. Kane, A. Ghosh et al., "Synthesis and soft magnetic properties of Zn0.8-xNixMg0.1Cu0.1Fe2O4 (x = 0.0-0.8) ferrites prepared by sol-gel auto-combustion method," *Journal of Alloys and Compounds*, vol. 615, no. 1, pp. 313–316, 2015.

[35] S. N. Kane and M. Satalkar, "Correlation between magnetic properties and cationic distribution of Zn0.85−x Ni x Mg0.05Cu0.1Fe2O4 nano spinel ferrite: effect of Ni doping," *Journal of Materials Science*, vol. 52, no. 6, pp. 3467–3477, 2017.

[36] K. Rajasekhar Babu, K. R. Rao, and B. Rajesh Babu, "Cu 2+ -modified physical properties of Cobalt-Nickel ferrite," *Journal of Magnetism and Magnetic Materials*, vol. 434, pp. 118–125, 2017.

[37] A. Hajalilou, H. M. Kamari, and K. Shameli, "Dielectric and electrical characteristics of mechanically synthesized Ni-Zn ferrite nanoparticles," *Journal of Alloys and Compounds*, vol. 708, pp. 813–826, 2017.

[38] M. A. Almessiere, Y. Slimani, M. Sertkol et al., "Ce-Nd Co-substituted nanospinel cobalt ferrites: an investigation of their structural, magnetic, optical, and apoptotic properties," *Ceramics International*, vol. 45, no. 13, Article ID 16147, 2019.

[39] M. P. Ghosh, S. Datta, R. Sharma, K. Tanbir, M. Kar, and S. Mukherjee, "Copper doped nickel ferrite nanoparticles: jahn-Teller distortion and its effect on microstructural, magnetic and electronic properties," *Materials Science and Engineering: B*, vol. 263, Article ID 114864, 2021.

[40] G. B. Huang, Q. Y. Zhu, and C. K. Siew, "Extreme learning machine: theory and applications," *Neurocomputing*, vol. 70, no. 1, pp. 489–501, 2006.

[41] A. Alqahtani, "Engineering the energy gap of cupric oxide nanomaterial using extreme learning machine and stepwise regression algorithms," *Journal of Nanomaterials*, vol. 2021, Article ID 4797686, 2021.

[42] X. Liu, Q. Ge, X. Chen, J. Li, and Y. Chen, "Extreme learning machine for multivariate reservoir characterization," *Journal of Petroleum Science and Engineering*, Article ID 108869, 205 pages, 2021.

[43] U. Safder, J. Loy-benitez, H.-T. Nguyen, and C. Yoo, "A hybrid extreme learning machine and deep belief network framework for sludge bulking monitoring in a dynamic wastewater treatment process," *Journal of Water Process Engineering*, vol. 46, Article ID 102580, 2022.

[44] O. E. Oyeneyin, B. S. Obadawo, A. A. Olanrewaju et al., "Predicting the bioactivity of 2- alkoxycarbonylallyl esters as potential antiproliferative agents against pancreatic cancer (MiaPaCa-2) cell lines," *GFA-based QSAR and ELM-based models with molecular docking*, vol. 19, 2021.

[45] Y. Li, Y. Zeng, Y. Qing, and G.-B. Huang, "Learning local discriminative representations via extreme learning machine for machine fault diagnosis," *Neurocomputing*, vol. 409, pp. 275–285, 2020.

[46] Y. Ma, L. Wu, Y. Guan, and Z. Peng, "The capacity estimation and cycle life prediction of lithium-ion batteries using a new broad extreme learning machine approach," *Journal of Power Sources*, vol. 476, no. 56, Article ID 228581, 2020.

[47] W. Ahmed, H. Ma, X. Ouyang, and D. Y. Mo, "Prediction of aircraft trajectory and the associated fuel consumption using covariance bidirectional extreme learning machines," *Transp. Res. Part E*, vol. 145, Article ID 102189, 2021.

[48] E. Han and N. Ghadimi, "Model identification of proton-exchange membrane fuel cells based on a hybrid convolutional neural network and extreme learning machine optimized by improved honey badger algorithm," *Sustainable Energy Technologies and Assessments*, vol. 52, Article ID 102005, 2022.

[49] S. M. I. Shamsah and T. O. Owolabi, "Modeling the maximum magnetic entropy change of doped manganite using a grid search-based extreme learning machine and hybrid gravitational search-based support vector regression," *Crystals*, vol. 10, no. 4, 310 pages, 2020.

[50] S. M. Sulaiman, P. A. Jeyanthy, D. Devaraj, and K. V. Shihabudheen, "A novel hybrid short-term electricity forecasting technique for residential loads using Empirical Mode Decomposition and Extreme Learning Machines," *Computers & Electrical Engineering*, vol. 98, Article ID 107663, 2022.

[51] T. O. Owolabi, "Extreme learning machine and swarm- based support vector regression methods for predicting crystal lattice parameters of pseudo-cubic/cubic perovskites Extreme learning machine and swarm-based support vector regression methods for predicting crystal lat," *Journal of Applied Physics*, vol. 127, Article ID 245107, 2020.

[52] M. Co, O. Fe, V. Verma, M. Kaur, and J. Marc, "Tailored structural, optical and magnetic properties of ternary nano-hybrid," *Ceramics International*, vol. 45, no. 8, Article ID 10865, 2019.

[53] N. Cu, C. Fe, A. Aslam et al., "Physica B: physics of Condensed Matter Study of structural, optical and electrical properties of La 3 + doped Mg 0.25," *Phys. B Phys. Condens. Matter*, vol. 602, Article ID 412565, 2021.

[54] N. Amin, M. S. Ul Hasan, Z. Majeed et al., "Structural, electrical, optical and dielectric properties of yttrium substituted cadmium ferrites prepared by Co-Precipitation method," *Ceramics International*, vol. 46, no. 13, Article ID 20798, 2020.

[55] S. B. Somvanshi, S. A. Jadhav, M. V. Khedkar, P. B. Kharat, S. D. More, and K. M. Jadhav, "Structural, thermal, spectral, optical and surface analysis of rare earth metal ion (Gd3+) doped mixed Zn-Mg nano-spinel ferrites," *Ceramics International*, vol. 46, no. 9, Article ID 13170, 2020.

[56] A. Aslam, A. U. Rehman, N. Amin et al., "Lanthanum doped Zn0.5Co0.5LaxFe2−xO4 spinel ferrites synthesized via co-precipitation route to evaluate structural, vibrational, electrical, optical, dielectric, and thermoelectric properties," *Journal of Physics and Chemistry of Solids*, vol. 154, Article ID 110080, 2021.

[57] P. A. Vinosha, A. Manikandan, R. Ragu et al., "Impact of nickel substitution on structure, magneto-optical, electrical and acoustical properties of cobalt ferrite nanoparticles,"

Journal of Alloys and Compounds, vol. 857, Article ID 157517, 2021.

[58] K. Hussain, N. Amin, and M. I. Arshad, "Evaluation of structural, optical, dielectric, electrical, and magnetic properties of Ce3+ doped Cu0.5Cd0.25Co0.25Fe2-xO4 spinel nano-ferrites," *Ceramics International*, vol. 47, no. 3, pp. 3401–3410, 2021.

[59] A. Tony Dhiwahar, M. Sundararajan, P. Sakthivel, C. S. Dash, and S. Yuvaraj, "Microwave-assisted combustion synthesis of pure and zinc-doped copper ferrite nanoparticles: structural, morphological, optical, vibrational, and magnetic behavior," *Journal of Physics and Chemistry of Solids*, vol. 138, Article ID 109257, 2020.

[60] Y. Slimani, H. Güngüne, M. Nawaz, A. Manikandan, H. S. El Sayed, and M. A. Almessiere, "Magneto-optical and microstructural properties of spinel cubic copper ferrites with Li-Al co-substitution," *Ceramics International*, vol. 44, Article ID 14242, 2018.

[61] N. Ghazi, H. Mahmoudi Chenari, and F. E. Ghodsi, "Rietveld refinement, morphology analysis, optical and magnetic properties of magnesium-zinc ferrite nanofibers," *Journal of Magnetism and Magnetic Materials*, vol. 468, pp. 132–140, 2018.

[62] H. Javed, A. Rehman, S. Mussadiq et al., "Reduced graphene oxide-spinel ferrite nano-hybrids as magnetically separable and recyclable visible light driven photocatalyst," *Synthetic Metals*, vol. 254, pp. 1–9, 2019.

[63] B. S. Yildiz and A. R. Yildiz, "Comparison of grey Wolf, whale, water cycle, ant lion and sine-cosine algorithms for the optimization of a vehicle engine connecting rod," *Materials Testing*, vol. 60, no. 3, pp. 311–315, 2018.

[64] N. Pholdee, S. Bureerat, and A. R. Yildiz, "Hybrid real-code population-based incremental learning and differential evolution for many-objective optimisation of an automotive floor-frame," *International Journal of Vehicle Design*, vol. 73, no. 1, pp. 20–53, 2017.

[65] S. Karagoz and A. R. Yildiz, "A comparison of recent metaheuristic algorithms for crashworthiness optimisation of vehicle thin-walled tubes considering sheet metal forming effects," *International Journal of Vehicle Design*, vol. 73, no. 1, pp. 179–188, 2017.

[66] N. M. Sabri, M. Puteh, and M. R. Mahmood, "A review of gravitational search algorithm," *International Journal of Advances in Soft Computing and Its Applications*, vol. 5, no. 3, 2013.

[67] R. Samala and M. Kotapuri, "Optimal DG sizing and siting in radial system using hybridization of GSA and Firefly algorithms," *Modelling, Measurement and Control A*, vol. 91, no. 2, pp. 77–82, 2018.

[68] O. E. Oyeneyin, B. S. Obadawo, D. S. Metibemu et al., "An exploration of the antiproliferative potential of chalcones and dihydropyrazole derivatives in prostate cancer via androgen receptor: combined QSAR, machine learning, and molecular docking techniques," *Phys. Chem. Res.*vol. 10, no. 2, pp. 211–223, 2022.

[69] O. Olubi, E. Oniya, and T. Owolabi, "Development of predictive model for radon-222 estimation in the atmosphere using stepwise regression and grid search based-random forest regression," *Journal of the Nigerian Society of Physical Sciences*, vol. 3, pp. 132–139, 2021.